Article

Capturing the Impact of 2018 European Drought and Heat Using OCO-2 Solar-Induced Fluorescence

Ankit Shekhar[1,3], Jia Chen[1,*], Shrutilipi Bhattacharjee[1], Allan Buras[2], Antony Oswaldo Castro[2], Christian S. Zang[2] and Anja Rammig[2]

[1] Technical University of Munich, TUM Department of Electrical and Computer Engineering, 80333 Munich, Germany; jia.chen@tum.de (J.C); Shrutilipi.bhattarcharjee@tum.de (S.B)
[2] Technical University of Munich, TUM School of Life Science Weihenstephan, 85354 Freising, Germany; allan@buras.eu (A.B); a.castro@tum.de (A.O.C); christian.zang@wzw.tum.de (C.S.Z); anja.rammig@tum.de (A.R)
[3] ETH Zurich, Department of Environmental Systems Science, 8092 Zurich, Switzerland; ankit.shekhar@usys.ethz.ch (A.S)
* Correspondence: jia.chen@tum.de;

Received: date; Accepted: date; Published: date

Abstract: The European heatwave of 2018 led to record-breaking temperatures and extremely dry conditions in many parts of the continent resulting in widespread decrease in agricultural yield, early tree-leaf senescence, and increase in forest fires in Northern Europe. Our study aims to capture the impact of the 2018 European heatwave on terrestrial ecosystem through the lens of a high-resolution solar-induced fluorescence (SIF) data acquired from the Orbiting Carbon Observatory (OCO-2) satellite. SIF is proposed to be a direct proxy for gross primary productivity (GPP) and thus can be used to draw inferences about changes in photosynthetic activity in vegetation due to extreme events. We explore spatial and temporal SIF variation and anomaly during spring and summer months across different vegetation types (agriculture, broadleaved forest, coniferous forest, and mixed forest) during the European heatwave of 2018 and compare it to non-drought conditions (most of Southern Europe). About one-third of Europe's land area experienced a consecutive spring and summer drought in 2018. Comparing 2018 to mean (2015-2017) conditions, we found a change in intra-spring season SIF dynamics for all vegetation types, with lower SIF during the start of spring followed by an increase in fluorescence from mid-April. Summer, however, showed a significant decrease in SIF. Our results show that particularly agricultural areas were severely affected by the hotter drought of 2018. Furthermore, the intense heat wave in Central Europe showed about 31% decrease in SIF values during July and August as compared to the mean over three previous years. Furthermore, our MODIS and OCO-2 comparative results indicate that especially for forests, OCO-2 SIF has a quicker response and possible higher sensitivity to drought in comparison to MODIS's fPAR and NDVI when considering shorter reference periods, which highlights the added value of remotely sensed solar-induced fluorescence for studying the impact of drought on vegetation.

Keywords: chlorophyll fluorescence, remote sensing, ecosystems, spring-summer, forest.

1. Introduction

Anthropogenic global warming is estimated to currently have reached about 1˚C above pre-industrial levels and is estimated to further increase to 1.5˚C between 2030 and 2052 under current rates of greenhouse gas (GHG) emissions [1]. This increase in global temperature is expected to lead to an increase in intensity and frequency of extreme events like heatwaves, drought and associated wildfires, [2–4]. In 2018, Europe faced such an extreme event characterized by record-breaking temperatures and long-lasting dryness, referred to as 'hotter drought' [5]. According to the European Drought Observatory of the European Commission, most of Northern and Central

 doi:10.20944/preprints202008.0327.v1

Europe was affected by such hotter drought in 2018. On the contrary, much of the Southern Mediterranean Europe experienced relatively cool and moist conditions [6,7]. For Central Europe, various news and media articles reported severe decrease in crop yields, increase in elderly mortality, and forest fires along with many other adverse impacts. According to a quick attribution study by the World Weather Attribution, [8] heat in Northern Europe, anthropogenic climate change has more than doubled the probability of occurrence of such a heatwave in the region.

Along with severe economic implications and adverse health impact on the public, such record-breaking hotter drought events severely affect ecosystems. A direct comparison of vegetation response to drought in 2018 and 2003 European heatwaves using MODIS's vegetation indices concluded that negative impacts in 2018 were even stronger than in 2003, with strong decline in agricultural land and forests, especially in Central Europe [6]. Such drought events strongly affect the carbon cycle, by leading to plant mortality and reductions in ecosystem carbon dioxide (CO_2) uptake, with the potential to convert ecosystems from carbon sinks into carbon sources [9,10].

Gross primary productivity (GPP) is a measure of ecosystem CO_2 assimilation. The estimation and modeling of regional or global GPP involves various uncertainties arising from model parameterization [11,12], thus demanding a more direct and reliable approach to estimate GPP. With recent advances in satellite-based measurements of solar-induced (chlorophyll) fluorescence (SIF), it is now possible to use SIF as a direct proxy for photosynthesis or GPP worldwide [13–17]. SIF is an electromagnetic signal emitted in the wavelength range of 600 to 800 nm by chlorophyll molecules [18]. Since SIF is directly associated with photosynthesis, it is more physiologically-based compared to the traditionally used vegetation indices (VIs) such as the normalized difference vegetation index (NDVI) and enhanced vegetation index (EVI) [19,20]. Over the last decade, several studies have demonstrated a strong linear relationship between satellite-based SIF and GPP [13,15,21–28], indicating that SIF might provide a useful approximation of GPP. The SIF retrievals obtained from the Japanese Greenhouse Gases Observing Satellite (GOSAT) and the European Global Ozone Monitoring Experiment-2 (GOME-2) were most widely used in the last decade (2007-2017; [24,28–31]). However, due to coarse spatial resolution of the SIF footprint (10 km diameter for GOSAT and 40 × 40 km^2, for GOME-2), these satellites presently impose serious limitations to detect eco-physiological changes across different vegetation types. The recent NASA's Orbiting Carbon Observatory-2 (OCO-2) satellite (launched September 2014) provides SIF data at a much higher spatial resolution of 1.3 × 2.25 km^2 with increased SIF acquisition frequency, thereby allowing to resolve SIF responses of various vegetation types under different climatic conditions [15,32].

SIF acquired from GOSAT and GOME-2 have been previously used to study the effect of drought on vegetation. Using GOSAT's SIF [33] showed that midday fluorescence explained the water stress over the Amazonian forests during a dry season in 2010. Yoshida et al [34] used GOME-2's SIF to study the impact of the 2010 Russian drought and highlighted the drought-related SIF decrease for croplands and grasslands. Sun et al [35] studied the drought onset mechanisms and its impact on agriculture using GOME-2 SIF during the droughts of 2011 in Texas and 2012 in the central Great Plains, United States. They concluded that SIF is sensitive to both structural and physiological variation in vegetation during drought and considered it an appropriate tool for drought monitoring. Koren et al [36] developed a GOME-2 based SIF product to show that spatial SIF response was in good agreement with meteorological (temperature, soil moisture, evapotranspiration and terrestrial water storage) anomalies during the 2015/2016 El Niño Amazon drought. Recently Zhang et al [37] constructed a global gridded SIF dataset (CSIF) using a neural network trained by OCO-2 and MODIS data, which they also employed for drought monitoring. Their preliminary result showed that CSIF well-captured the spatial extent of droughts during the 2015 European heatwave.

Here, we present the impact of the 2018 European hotter drought on terrestrial ecosystem as perceived through OCO-2 SIF data. The novelty of this study is highlighted through the detection

 doi:10.20944/preprints202008.0327.v1

of spatial and temporal patterns of OCO-2 SIF responses to drought and heat across different vegetation types. We captured and analyzed the spring-summer seasonal variation and anomaly in chlorophyll fluorescence across different vegetation types and tracked it with VPD and temperature anomalies. Furthermore, we compare SIF responses of different vegetation types under drought and non-drought conditions in Europe to explore the ability of OCO-2 SIF for drought impact characterization. Furthermore, we also discuss and compare our results with recent MODIS-based NDVI drought impact study. Finally, we discuss the drought-induced changes in satellite-based SIF measurements and perspectives of OCO remote sensing satellite products for future studies.

2. Materials and Methods

2.1 Study area

The study area is restricted to the European Union. About 1/3rd of Europe (1.8 M km^2, drought area, Figure 1(a-c)) was under consecutive spring (March-May) and summer (June-August) meteorological drought (drought area) according to the widely accepted standardized precipitation evapotranspiration index (SPEI) [38] (Figure 1 (a-c)). Also, from mid-July to mid-August, Central Europe was affected by heatwaves with temperatures more than 5°C higher than average for more than a week (NOAA Global Climate Report – July, August 2018; [39,40]). These drought and heat conditions resulted in a severe decline in agricultural yields and early leaf senescence and forest fires across Central and Northern Europe. At the same time, about 1/3rd of Europe (2 M km^2, non-drought area, Figure 1 (a-c)) experienced non-drought (i.e., normal or wet) conditions during spring and summer, mostly across the Mediterranean (Figure 1(a-c)). Although during summer, Spain and Portugal did experience record-breaking temperatures, above normal precipitation prevented drought conditions to prevail. Thus, Europe in 2018 provides us the opportunity for a comparative study between productivity under consecutive spring-summer drought and under non-drought conditions.

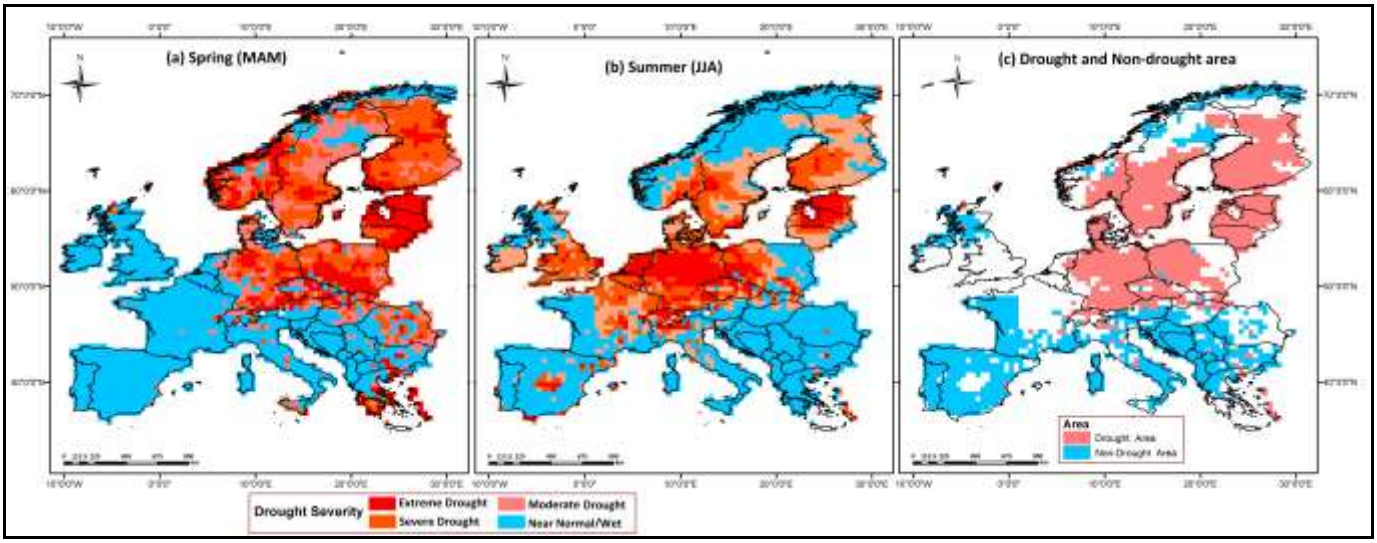

Figure 1. Drought severity map of Europe in (a) spring and (b) summer of 2018. The map is based on the SPEI Global Drought Monitor (http://spei.csic.es/index.html). (c) Drought area and non-drought area used in the study. Drought area has 2018 spring and summer SPEI values less than -1. Non-drought area has 2018 spring and summer SPEI values greater than -1.

2.2 Description of datasets

2.2.1 SIF data

 doi:10.20944/preprints202008.0327.v1

Light energy absorbed by the leaf chlorophyll molecules has three different pathways: photochemistry, non-photochemical quenching (NPQ, i.e., heat dissipation), and a small fraction re-emitted as SIF [18].Theoretically, SIF can be expressed as shown in Equation 1 [22].

$$SIF = APAR \times \Phi_F \times \Omega_C = PAR \times fPAR \times SIF_{yield} \quad (1)$$

where APAR is the absorbed photosynthetically active radiation in Watts/m^2, which is the product of photosynthetically active radiation (PAR) and the fraction of photosynthetically active radiation absorbed (fPAR) by the vegetation/canopy. SIF_{yield} is the emitted SIF per photon absorbed [17] and is also defined as the effective fluorescence yield of the canopy. SIF_{yield} is the product of fluorescence yield in the wavelength band of measurement (Φ_F) and an escape probability term (Ω_C). SIF_{yield} is expected to vary with the plant's photosynthetic light use efficiency [41,42] and canopy structural characteristics like leaf area index (LAI). However, with a satellite-based SIF measurement it is challenging to separate the canopy physiological (Φ_F) and structural components (Ω_C) from SIF_{yield} [35,43] and it is still an active area of research.

For this study, the SIF product from NASA's OCO-2 satellite was used since other satellite-based SIF retrievals were of coarser spatial resolution (GOSAT and GOME-2). OCO-2 SIF is made available by the CO2 Data Portal managed by the Jet Propulsion Laboratory of the California Institute of Technology, United States (https://co2.jpl.nasa.gov/). The OCO-2 spectrometer measures spectra in the O_2-A band (757–775 nm, full width at half maximum = 0.042 nm), with far-red SIF, retrieved at 757 and 771 nm based on the infilling of Fraunhofer lines [32,44]. The SIF retrieved at 771 nm is typically about 1.5 times smaller than obtained at 757 nm [44], therefore we utilized SIF retrieved at 757 nm in our study. The major advantage of OCO-2 SIF include an about 100-fold increase in data acquisition frequency over GOSAT and finer spatial resolution (1.3×2.25 km^2). This enables OCO-2 to acquire more than 10^5 clear-sky soundings on land per day, thus providing the opportunity to perform in-depth SIF based analysis like regional eco-physiological change detection [45,46]. However, OCO-2 SIF soundings do not have full spatial coverage (Figure 2). In this study, the SIF retrievals from the Level-2 OCO-2 Lite product, data version SIF v8 (version 8) were used from their first availability (6th September 2014) to 1st October 2018 for the whole European continent. The OCO-2 Lite product is bias-corrected and contains only good quality SIF sounding [47]. The OCO-2 takes measurements in three different observation modes, namely nadir, glint viewing, and a special target mode with different viewing zenith angle (VZA), typically alternatively with a repeat cycle of 16 days. Although SIF values are affected by VZA [48], grouping all the SIF sounding over a large area results in no significant SIF difference in the mean SIF between nadir and the combined modes [13,16] (please see Appendix A, table A1). In this study, we used SIF sounding from only nadir and glint mode, which each mode contributing about half of the total number of soundings. The percentage of nadir and glint mode data was consistent throughout the study period (Table S2). Figure S1 illustrates the trajectory and spatial distribution of the SIF soundings for Europe in 2018. The OCO-2 is a sun-synchronous satellite with a local overpass time at 1:30 PM compared to 9:30 AM for GOME-2 and 1:00 PM for GOSAT, thus compared to GOME-2, it better captures the sensitivity of fluorescence yield to water stress which is higher in the afternoon when plant water stress tends to peak [49]. Two important environmental factors that regulate plant photosynthesis are temperature and vapor pressure deficit (VPD). The SIF Lite data files also included VPD and temperature data from ECMWF for each SIF measurement.

2.2.2 MODIS data

Theoretically, SIF is directly related to fPAR (Equation 1). Thus, for improving the interpretation of SIF variation and anomalies, we used the MODIS Aqua fPAR product (MYD15A2H) version 6 [50,51], which is an 8-day composite data set with a spatial resolution of 500 meters covering the same period as OCO-2 SIF dataset. The fPAR calculation is based on 3D radiative transfer equation

(Look-Up-Table based approach, [52]), which takes 'best' quality spectral information of red and near-infrared band within the 8-day period as an input, and a back-up algorithm uses empirical relationship based on NDVI. In addition, we also used the standard MODIS 16-days composite NDVI product [53] with a spatial resolution of 250m, from Terra (MOD13Q1) and Aqua (MYD13Q1) for comparison with SIF. These composite products are constructed using the 'best' quality pixel (low clouds, low view angle and highest NDVI) over the 16 days period of Terra and Aqua measurements [53]. The MODIS products were obtained from the NASA Land Processes Distributed Active Archive Center (LP DAAC, https://lpdaac.usgs.gov/products). Moreover, only good quality MODIS pixels (VI Quality variable = 0, indicating good quality as per [53]) for fPAR and NDVI were chosen for subsequent analysis.

2.2.3 Corine Land Cover data

To study the SIF variation across different vegetation types (agriculture, broadleaved forest, coniferous forest, and mixed forest), we used the most recent Corine Land Cover (CLC) 2018, Version 20b2 provided by the European Environmental Agency (EEA) (Figure S2). The CLC 2018 uses Sentinel-2 and Landsat-8 imageries for its construction, thereby achieving a minimum mapping width (resolution) of 100*100 m (CLC2018 Technical Guidelines, 2017;[54]). Agricultural land comprising arable lands, pastures, and heterogeneous agricultural area covered most of the parts of drought area (53%) and non-drought area (57%), followed by coniferous forest of about 37% in the drought area (Table S1).

2.3 Data analysis

The gridded SPEI data for spring (March, April, and May, MAM) and summer (June, July, and August, JJA) was obtained from the SPEI Global Drought Monitor (http://spei.csic.es/index.html). The drought areas were defined as the areas which showed SPEI less than or equal to -1 (meteorological drought conditions) for both spring and summer season [55,56], whereas the non-drought areas were the ones with SPEI > -1 (near normal and wet conditions, or non-drought conditions) for both spring and summer.

Standardized meteorological based drought indices can sometimes misrepresent actual climatic water balance (CWB) [57]. The SPEI<-1 values for the study area in 2018 completely indicated water deficit conditions with negative CWB values during the summer season (Figure S3). Figure 1c shows the drought and non-drought area used in this study. Thereafter, OCO-2 SIF sounding data for the drought and non-drought area were spatially joined to the CLC based on geographic intersection (intersection of SIF sounding and the CLC polygons). To study the variation of SIF across the drought and non-drought areas in spring and summer for Europe, we spatially aggregated all the daily SIF soundings for each of the above described vegetation types separately for drought and non-drought areas over the spring and summer season.

SIF changes because of two reasons; firstly due to natural seasonal vegetation change during the growing season (e.g. change in chlorophyll content during the seasonal cycle) and secondly due to stress (e.g., heat and drought stress). To study the inter- and intra-seasonal SIF variation and anomalies during the drought in spring and summer, we compared SIF, temperature and VPD of 2018 (SIF_2018, Temp_2018, VPD_2018) with their average (mean of 2015-2017; SIF_Mean, Temp_Mean, VPD_Mean) on a 5-day running average [9]. These anomalies of the average SIF at a given date would eliminate the SIF changes due to seasonality. It is important to note that Central Europe suffered from a heat wave during summer of 2015, with record high temperatures and precipitation deficit [58,59], which may lower our detected impact of 2018. For each OCO-2 footprint, co-located MODIS's NDVI and FPAR was interpolated in time and space so that the same sample is used for each data set. Finally, the OCO-2 SIF was spatially (Drought area) and temporally (8-day) aggregated to compare with NDVI and fPAR.

 doi:10.20944/preprints202008.0327.v1

We performed a Wilcoxon-rank sum test [60] to test for a significant location-shift (i.e. the non-parametric difference of means) between the SIF_2018 and SIF_Mean. SIF, temperature and VPD anomalies (SIF-diff, Temp-diff and VPD-diff) were defined as differences between 2018 and average (for e.g. SIF-diff = SIF_2018 – SIF_Mean). With continued drought condition during the summer, Central Europe also experienced an intense heatwave during late July to early August, 2018. The heatwave was pronounced in Belgium (BEL), Netherlands (NLD), Denmark (DEN) and Germany (DEU) according to the reports published by the Royal Meteorological Institute of Belgium [61], Royal Netherlands Meteorological Institute [62], Danish Meteorological Institute [63] and the German Meteorological Office [64], respectively. To quantify the impact of this heatwave, SIF soundings of BEL, NLD, DEN and DEU from 15th July to 15th August, 2018 were analyzed for all the vegetation types and compared to the mean of 2015-2017. All analyses were processed in 'R'[65], extended by the packages stats, ggplot2 [66] and dplyr [67].

3. Results

3.1 Overall spring-summer SIF variation and anomaly

Overall, the whole of Europe showed average SIF_2018 values of 0.642 W/m²/sr/μm compared to SIF_Mean of 0.670 (Table 1a) during spring and summer season. Although, the SIF anomaly (SIF-Diff) was not significant for spring and combined spring-summer season for drought areas (Fig S1), and the whole of Europe, the summer season showed a significant decrease (p-value < 0.001) in SIF_2018 compared to SIF_Mean in the drought area (Table 1; Figure 2). The pattern of combined spring-summer season SIF-Diff for drought and non-drought area (Figure 1c) were complementary to each other (Table 1a). Also, the drought areas showed positive SIF-Diff for spring and negative SIF-Diff for summer and combined spring-summer season, whereas the non-drought area showed positive SIF-Diff for spring and combined spring-summer season. Although most of the SIF-Diff was not significant (p-value > 0.05), it is however interesting to see a distinct pattern between seasonal variability of SIF in relation to drought.

Table 1. European-wide mean SIF_757nm (W/m²/sr/μm) values in spring, summer and combined spring-summer season and their corresponding anomaly (SIF-Diff) for whole of Europe, drought area and non-drought area.

	(a) Combined spring-summer			(b) Spring			(c) Summer		
Area	**SIF_2018**	**SIF_Mean**	**SIF-Diff**	**SIF_2018**	**SIF_Mean**	**SIF-Diff**	**SIF_2018**	**SIF_Mean**	**SIF-Diff**
Europe	0.642	0.670	-0.028	0.523	0.534	-0.011	0.766	0.820	-0.054*
Drought area	0.558	0.596	-0.038	0.407	0.388	0.019	0.711	0.814	-0.103*
Non-drought area	0.684	0.660	0.024	0.601	0.560	0.041	0.766	0.767	-0.001

* p-value < 0.001

Preprints (www.preprints.org) | NOT PEER-REVIEWED | Posted: 14 August 2020 doi:10.20944/preprints202008.0327.v1

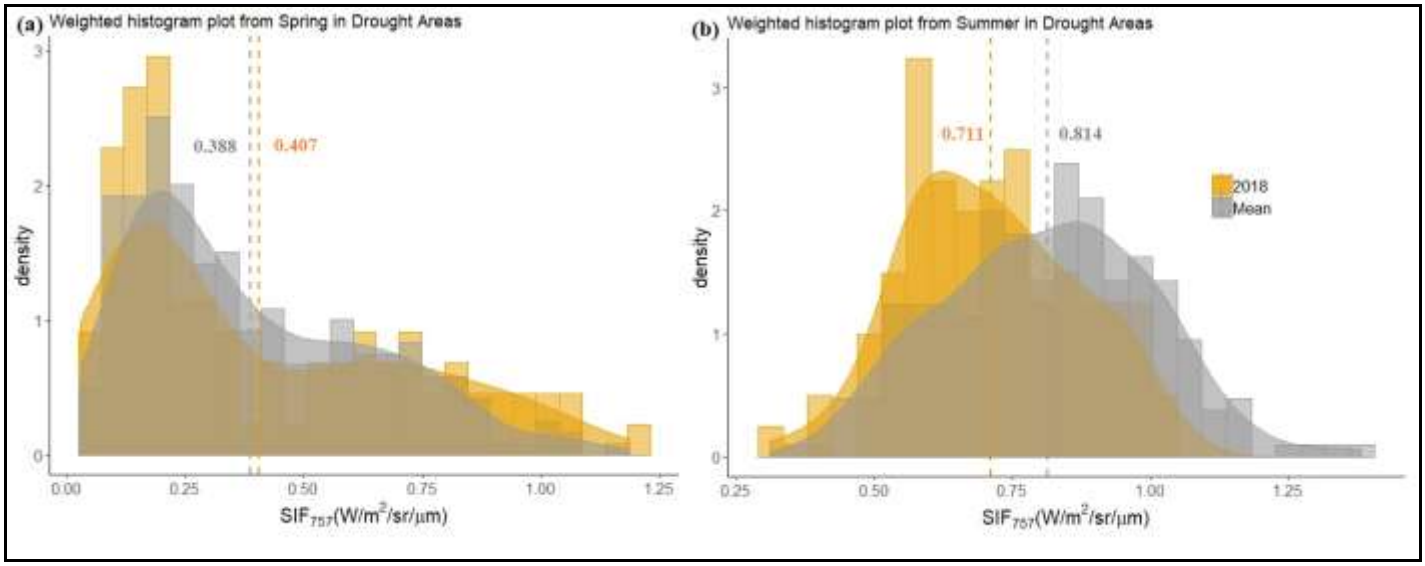

Figure 2. Overall SIF variation in (a) spring and (b) summer season for drought areas in 2018 (SIF_2018, in orange) compared to mean SIF values from 2015-2017 (SIF_Mean, in grey). Bars indicate the histogram of the SIF, whereas curves represent the density plot of the histogram.

3.2 Intra-seasonal SIF variation and anomalies for different vegetation types

The drought area was characterized by higher temperatures during the second half of both spring and summer season (Figure 3b). For the drought area, SIF-Diff was initially significantly negative at the start of the spring season for the agricultural area, whereas the difference was not significant for forests. Here, significance is considered as a departure of (SIF/fPAR/NDVI) values > 1 standard error [34,35], i.e., for Figure 3a, when the blue and red shades are not overlapping. However, with increase in Temp-Diff and VPD-Diff from a couple of weeks after the middle of spring season (DOY 120), SIF-Diff significantly increased across all land cover types (Figure 3a and 3b), with SIF-Diff values as high as 0.25, 0.65, 0.25 and 0.4 W/m2/sr/µm for agricultural area, broadleaved, coniferous, and mixed forests, respectively. The broadleaved forests (BLF) in the drought-area occur across a large range of latitude (from 45 N in Germany to 70 N in Norway; Figure S2) and Köppen climate zones (warm summer and cool summer). More intense and early spring warming occurred in the warm summer climate, whereas a moderate and later warming occurred in the cool summer climate zone (blue and black line in Figure S6). This seems to have caused leaf flushing (represented by the blue and green box in S6) at a difference of about 20 days between the two climate zones. Now, since our result is spatially and temporally aggregated, this shows two peaks during the spring for BLF. Thus, although there was no overall change in SIF for the spring season (section 3.1), we observed a change in the intra-spring SIF variation pattern in 2018 compared to the mean, with an initial decrease (March to April) followed by a significant increase in SIF in May. This intra-spring SIF variation reflected in fPAR variations during the spring season for drought area (Figure A1). Thus, SIF variation in spring was strongly related to fPAR for drought areas where continuous higher temperature and VPD were observed in the second half of the spring season (April-May). The summer season of 2018 was characterized by negative SIF-Diff (Figure 3) especially for agricultural areas which showed continuous negative values throughout the summer season (Figure 3). For forest areas, however, we observed significantly negative SIF-Diff only in the later part of summer (from July, DOY 185-215) when the temperature values were more than 5 degrees higher than the mean (Figure 3b).

The non-drought areas were characterized by significantly higher temperatures only during the end of April (DOY 105-120) as illustrated in Figure 4b. Here, we observed the spring variation to be similar to that of the drought area (Figure 4a and 4b), which is also visible in the fPAR data (Figure S4a). In contrast to the drought area, summer in the non-drought area featured positive SIF-Diff for

Preprints (www.preprints.org) | NOT PEER-REVIEWED | Posted: 14 August 2020 doi:10.20944/preprints202008.0327.v1

all the vegetation types and especially for the agricultural area. For the non-drought area, fPAR in summer was higher than the mean value (Figure S4a) and also seems to closely relate to the SIF variation.

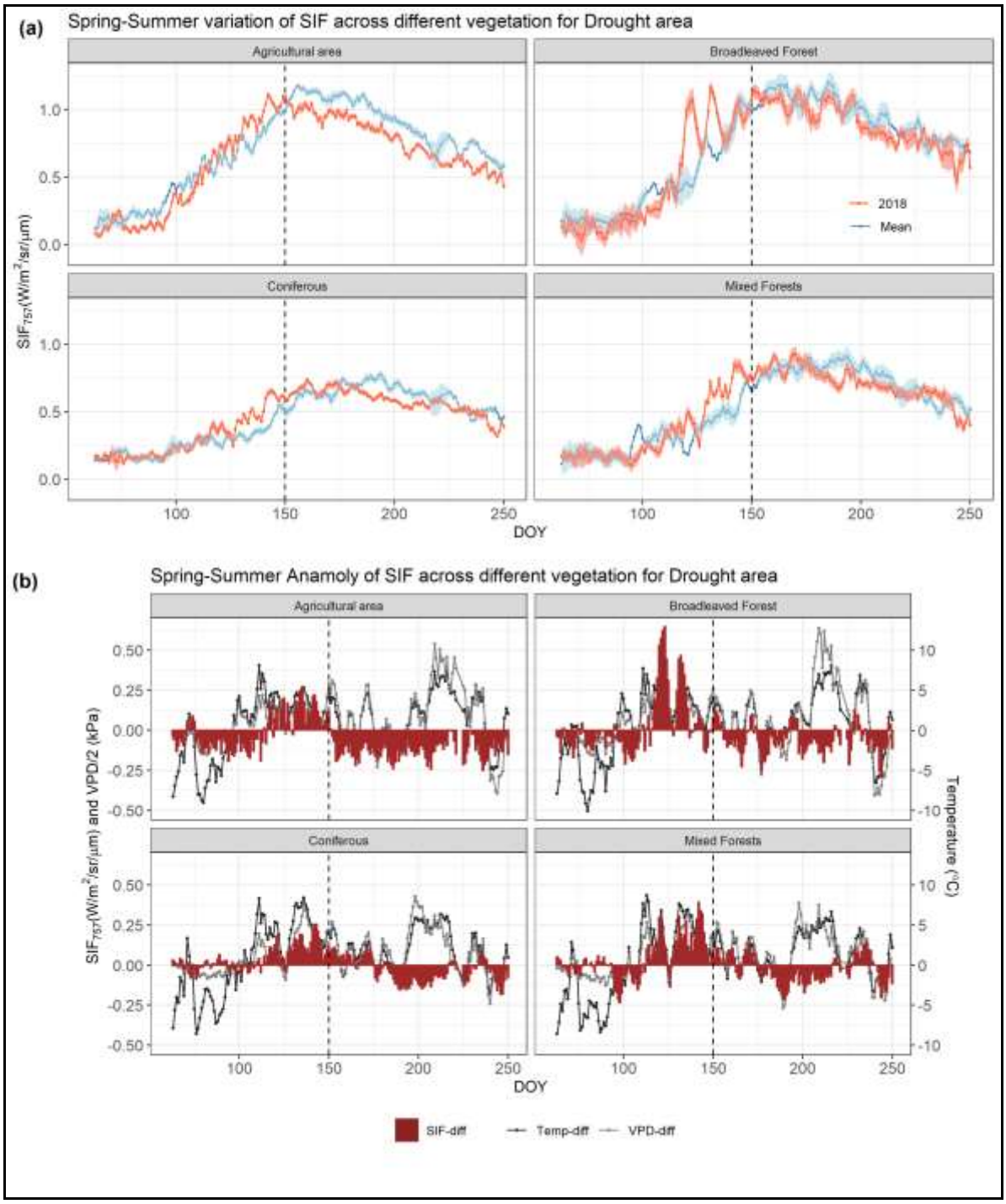

Figure 3. (a) Intra-seasonal SIF variability based on a 5-day running mean for drought areas across different vegetation types, (b) Corresponding SIF anomalies (SIF-Diff), and VPD (gray line) and temperature (black line) anomalies. Positive values indicate a surplus of SIF, Temp and VPD, negative values indicate lower values in comparison to the mean from 2015-2017. Shaded area (lightblue for 'Mean'; red for '2018') in part (a) is ± standard error of mean obtained after spatially aggregating the samples. The vertical dashed lines divide the DOY into spring (DOY 60-150) and summer (DOY 151-245) season. Temp-Diff = Temp_2018 – Temp_Mean; VPD-Diff = VPD_2018 – VPD_Mean.

Preprints (www.preprints.org) | NOT PEER-REVIEWED | Posted: 14 August 2020 doi:10.20944/preprints202008.0327.v1

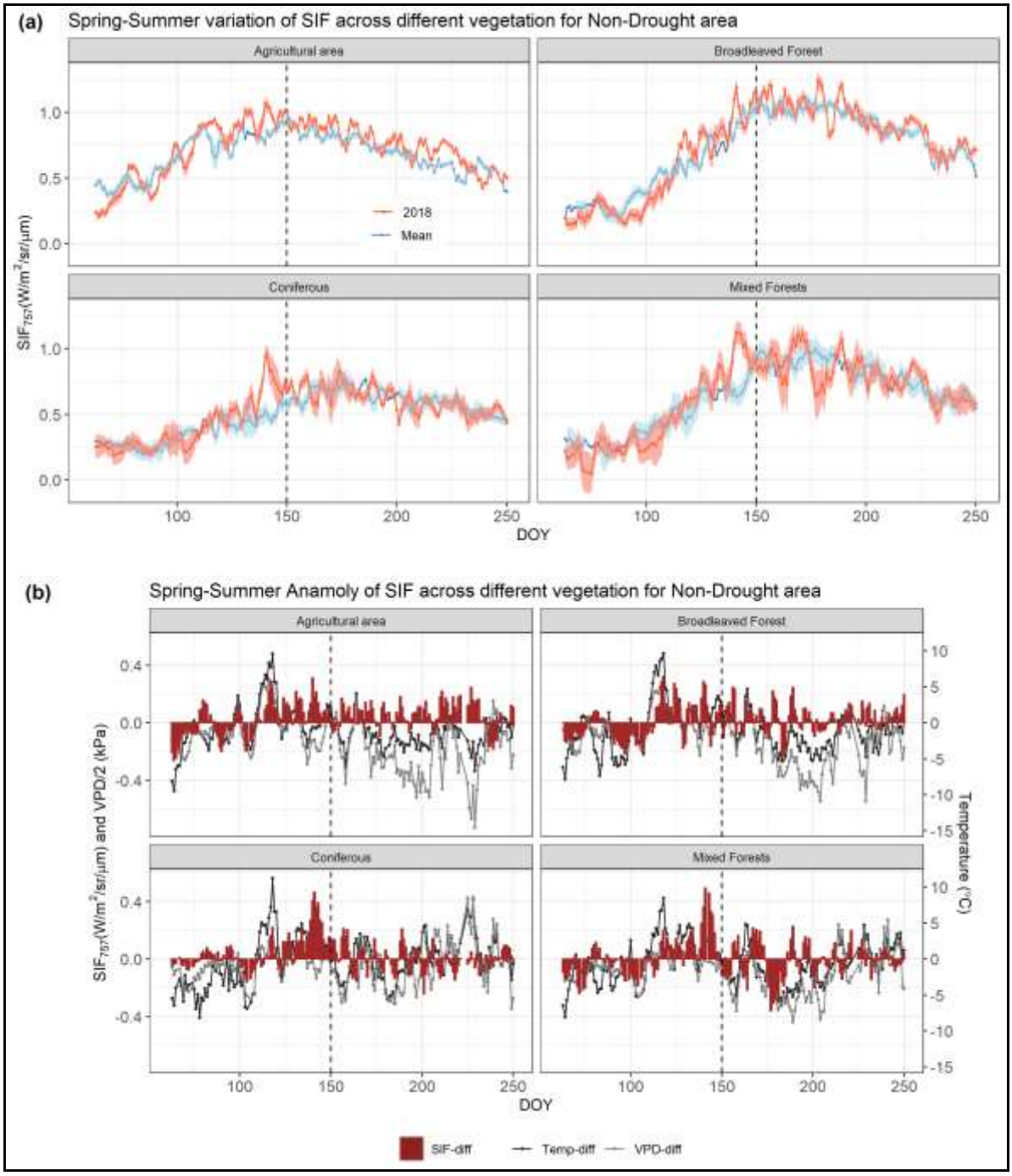

Figure 4. (a) Intra-seasonal SIF variability based on 5-day running mean for non-drought areas across different vegetation types, (b) (b) Corresponding SIF anomalies (SIF-Diff), and VPD (gray line) and temperature (black line) anomalies. Positive values indicate a surplus of SIF, Temp and VPD, negative values indicate lower values in comparison to the mean from 2015-2017. Shaded area (lightblue for SIF_Mean; red for SIF_2018) in part (a) is ± standard error of mean obtained after spatially aggregating the samples. The vertical dashed lines divide the DOY into spring (DOY 60-150) and summer (DOY 151-240) season. Temp-Diff = Temp_2018 – Temp_Mean; VPD-Diff = VPD_2018 – VPD_Mean.

3.3 SIF variation during the heatwave

Apart from the extensive drought conditions, Central Europe was also largely affected by the 2018 heatwave, which was characterized by unusually high temperature anomalies (+5-8 °C) from mid-July to mid-August (Figure 3a). Overall, during this heatwave in Central Europe, the SIF_2018 was 31% lower than SIF_Mean. This difference was most pronounced in agricultural areas which

Preprints (www.preprints.org) | NOT PEER-REVIEWED | Posted: 14 August 2020 doi:10.20944/preprints202008.0327.v1

showed 34% lower SIF_2018 followed by mixed forest (25%), coniferous (22%) and broadleaved forest (16%) (Figure 5).

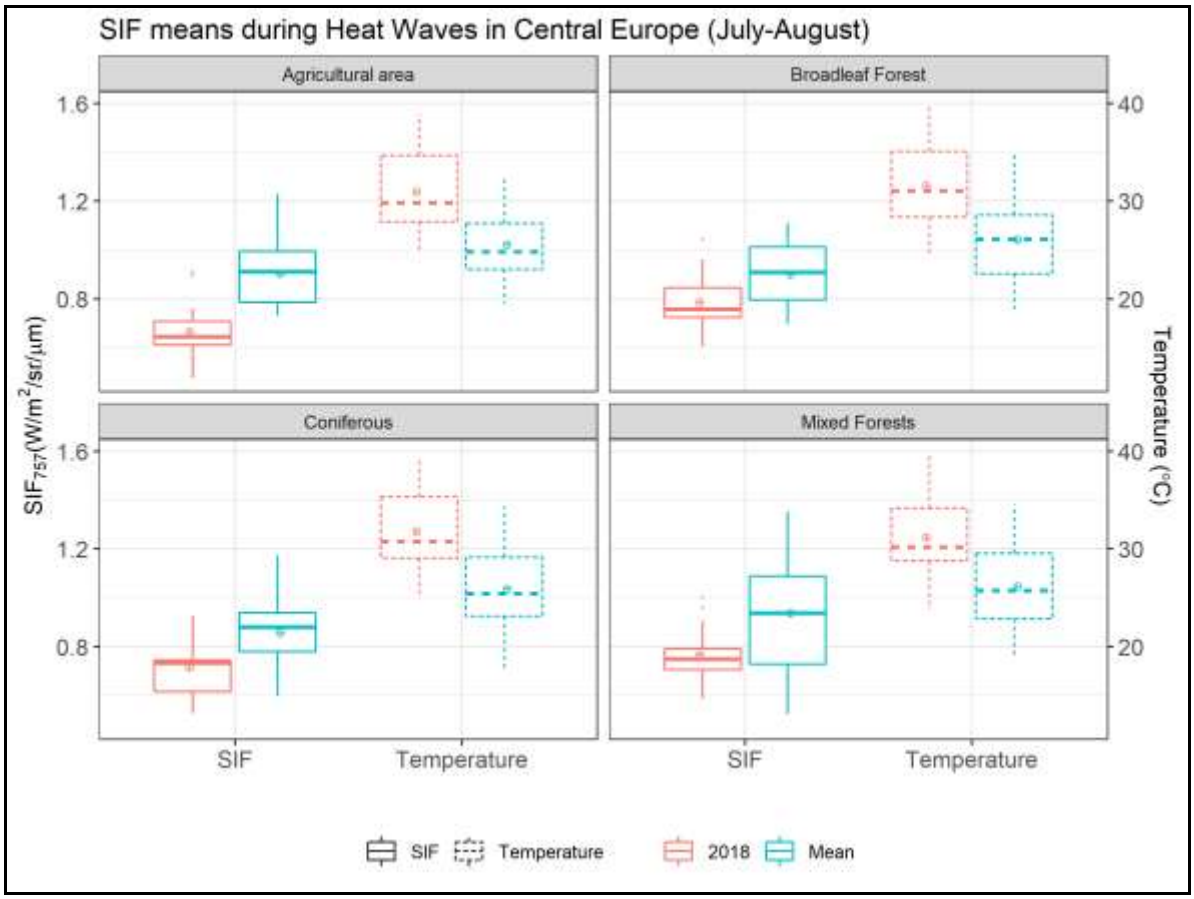

Figure 6. Boxplots illustrating SIF variation across the four vegetation type during the heatwave (15th July to 15th August) in central Europe (Germany, Denmark, Belgium and Netherlands) along with temperature differences. Dots inside the boxplots represent the corresponding mean values.

4. Discussion

4.1 Drought impact on SIF

Our study showed a clear impact of the European hotter drought of 2018 on overall and intra-seasonal SIF variation for different vegetation types as captured by the OCO-2 SIF. Early spring of 2018 was characterized by lower than average temperatures and VPD (non-stressed stage) followed by above average temperatures and VPD in the later part of spring (April-May; Figure 3b). Such cooler and wetter conditions in early spring can result in poor crop development and lower productivity [68] and thus, lower SIF values ([69]; Figure 3b). Moreover, the initially cooler conditions in spring might have delayed the leaf flushing in deciduous trees, resulting in lower SIF values of broadleaved forests (Figure 3b). This pattern was less evident for the coniferous and mixed forests, probably due to the presence of evergreen trees. Also, the wet conditions during early spring most likely built up enough soil moisture for the later spring season, thus moderating the sudden warming in later spring season [70,71]. This combination of ample moisture supply with a rise in temperature resulted in an increase in SIF to above average values across all vegetation types (Figures 3 and 6). The variation in SIF depends on the variation of both APAR (and fPAR) and SIF_{yield} (Equation 1,[72]). Both, SIF and fPAR were increasing during the spring season for both drought and non-drought areas (Figures 3, 4, A1a and S4). Moreover, for agriculture areas affected by

 doi:10.20944/preprints202008.0327.v1

drought, the peaks of fPAR and SIF were on almost the same day of the year (DOY ~ 145; Figure 3a and A1a). However, this clear synchronicity was not found for forests. Nevertheless, we conclude that the satellite-based SIF variation was closely coupled with fPAR variation under non-stress conditions (spring for drought areas and for non-drought areas in spring and summer). Previous studies [13,34,35] have also highlighted the synchronicity of satellite-based SIF with fPAR.

The warming during late spring continued to the summer season, with the later summer season featuring intense heat. We found decreasing SIF in all investigated vegetation types in summer of 2018, which was most pronounced in the drought areas. The agricultural areas expressed an immediate decrease in SIF from early summer onwards most likely because of severe soil moisture deficits caused by early water depletion in late spring in course of dry weather conditions [73,74]. Ongoing drought conditions during the summer season showed continuous decrease in SIF for agricultural area and, with some delay in forests (Figure 3). Similar findings were reported by an NDVI-based study where agricultural areas and, with some delay, forests in central Europe faced severe decline in NDVI during the summer season [6]. Unlike agricultural crops, forests feature a buffered micro-climate [75–77] and given their deeper rooting system in comparison to crops, have access to deeper soil water and thus, can maintain constant photosynthesis rates for extended periods during drought conditions [78].

Our spring-summer seasonal variation of SIF in 2018 is in close agreement with the one of MODIS NDVI ([6]) for agricultural areas. However, for the forest ecosystems, we found a less extreme SIF decline compared to NDVI-decline in Buras et al [6]. To further evaluate this difference we analyzed MODIS NDVI over 4 years (2015-2018), and our results indicate that SIF showed higher sensitivity compared to NDVI over the 4 years period (Figures A1b and 6). We observed that for the forest ecosystems in the drought area, fPAR- and NDVI-anomalies were positive during the summer season (DOY < 215) (Figures A1b and 6), i.e. when the SIF-anomaly was reportedly negative. While Buras et al [6] used a reference period spanning 2000-2018, where several normal and even moist summers were observed, the analyses presented here rely on the period 2015-2017 due to the comparably shorter mission length of OCO-2. However, in 2015 another severe drought hit central and southern Europe which might have resulted in forest legacy effects [79], i.e. low productivity and die-back in affected areas in 2016 [80]. Consequently, regarding forests, the fPAR and NDVI values from 2018 do only marginally differ to the period mean (2015-2017) since forests could have been suffering at least in 2015 and 2016, i.e. in 2 of the three years included in the reference mean. It is therefore not surprising that the extremeness of 2018 in the 4 year NDVI analysis of forests (Figures A1 and 6) did not capture the forest decline as clear as in Buras et al [6] (with 19 years reference period) where the majority of reference years represent years with sufficient water supply. In contrast to NDVI over the four years period, SIF was considerably lower in 2018 compared to the already low mean of previous three years (2015-2017) which may indicate its higher sensitivity to both physiological and structural drought response from plants. This finding highlights the predominance of SIF over NDVI if only short reference periods are available, for example, SIF available from OCO-2, upcoming OCO-3, and TROPOMI in comparison to SENTINEL (for NDVI).

Vegetation indices (VIs), such as NDVI are sensitive to canopy structure and pigment concentration with no direct link to photosynthesis [81]. This might lead to reduced sensitivity of these VIs to capture drought impact when the vegetation, such as high density forests, still remains green (no changes in chlorophyll content) but reduce their photosynthesis initially during heavily stressed drought conditions [82] in early summer during the European hotter drought. Similar conditions might also not have resulted in significant differences of NDVI during the early summer of 2018 from the mean (Figure A1b). Alternatively, higher sensitivity

Preprints (www.preprints.org) | NOT PEER-REVIEWED | Posted: 14 August 2020 doi:10.20944/preprints202008.0327.v1

of SIF (with direct links to photosynthesis) to drought impact on high density European forest was evident from our study (Figures 3 and 6).

The intense heatwave in Central Europe during July and August resulted in a significant decrease in SIF across all the four vegetation types, which was particularly pronounced for agricultural areas. The heatwave occurred at the end of the already dry summer, which was preceded by a dry spring. As a consequence of persisting drought, many crops desiccated, thus not emitting any fluorescence by end of July when temperatures were extremely high in Central Europe. Water stress due to high-temperature anomalies during a drought event can further increase heat stress due to an extended period of stomatal closure and subsequent reduction in evaporative cooling [83], thus causing positive feedback resulting in even warmer conditions [84].

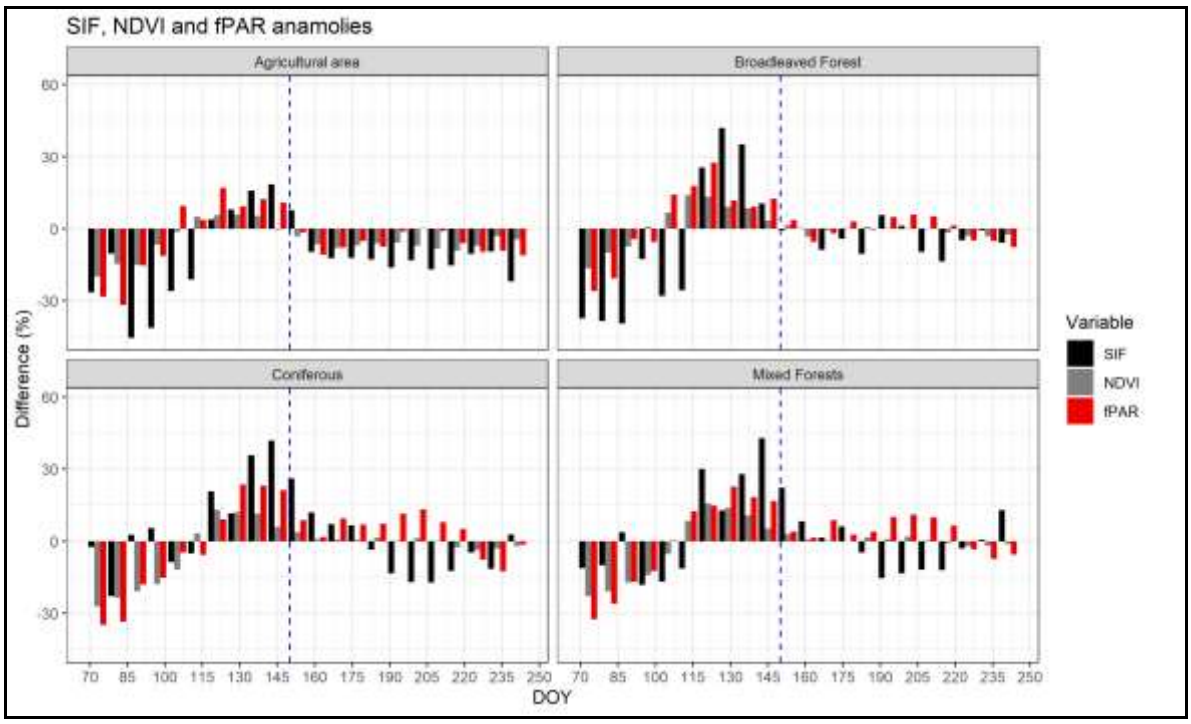

Figure 6. Anomalies (in % difference from 'Mean') of SIF, NDVI and fPAR for drought area across different vegetation types as observed from OCO-2 SIF, MODIS NDVI product (MOD/MYD13Q1) version 6 and MODIS fPAR product (MYD15A2H) version 6 in 2018. Positive values indicate a surplus of SIF, NDVI and fPAR, negative values indicate lower values in comparison to the mean from 2015-2017. The left and right side of blue vertical dashed line represents spring and summer season, respectively.

4.2 SIF response during drought stress

Water stress adversely impacts photosynthesis, either physiologically or structurally [85]. Physiological alterations include change in leaf biochemistry via reductions in enzymatic activity [86] or a reduction in mesophyll/chlorophyll, and stomatal conductance [87], resulting in lower CO_2 uptake by the plants and thus reduced photosynthesis (i.e. lower SIF values). The structural changes include foliar changes like leaf wilting or rolling (changes in leaf inclination), thus reducing effective leaf area index (LAI), which in turn causes a reduction in fPAR and energy available for photosynthesis and fluorescence emission [88,89]. Furthermore, plants adopt different mechanism to minimize water and heat stress, like chloroplast avoidance movement during which plants move their chloroplast from the cell surface to side walls of cell [90] so as to minimize APAR [91] and thus SIF. MODIS fPAR decrease due to these protection mechanism, and physiological and structural changes was visible for agricultural

 doi:10.20944/preprints202008.0327.v1

area during the summer drought (Figures A1 and 6). However, for the forest areas we found that MODIS fPAR for drought areas during mid-summer (DOY 185-215) was not lower than fPAR in previous 3 years (Figures 7 and 8). This might imply that reduction of SIF is likely caused by a reduction in SIF_{yield}. SIF variation due to changes in SIF_{yield} can be because of canopy's physiological (Φ_F term of Equation 1) or structural change (Ω_C term of Equation 1) or both. The PAR absorbed by leaves is partitioned into photochemistry, heat dissipation (NPQ) and fluorescence emission (SIF). Although fPAR (or APAR) did not decrease, the proportion of fPAR (or APAR) that is used in photochemistry (to drive electron transport for carbon assimilation) decreases, resulting in a surplus of photosynthetic energy. Now, two other pathways compete to de-excite the absorbed light that is not used in photochemistry (the surplus photosynthetic energy), the energy emitted as SIF or energy dissipated as heat through NPQ [72]. The competition between these two pathways depends on the environmental stress [92], and during water stress conditions (drought) the reduction in SIF is linked to higher NPQ [93,94]. This increase in NPQ may result in a weak coupling between SIF and fPAR under water stress conditions, which seems to be visible for forests during mid-summer (DOY 185-215; Figure A1). It is also possible that the MODIS fPAR could be erroneous [35] and not be the best estimate of fPAR, especially in case of high vegetation density (as in Europe). The backup algorithm of MODIS fPAR rely on its relationship with NDVI [52], which becomes non-linear with sharp drop of NDVI sensitivity to fPAR for moderate to high vegetation density for fPAR values beyond 0.7 (Figure S5). Nevertheless, further research to differentiate the canopy escape term (Ω_C term of Equation 1) from SIF (as demonstrated by [95,96]) to study changes in fluorescence yield (Φ_F) during extreme large scale drought event is recommended.

Our results highlight one more reason why OCO-2 SIF can be useful to study drought impact on vegetation as different vegetation types have different response to drought, which was not efficiently captured for each vegetation types before because of the coarser resolution of preceding satellite-based SIF products. We would like to stress, that earlier studies used SIF at coarser spatial resolution (from GOME-2 or GOSAT) and mostly were not able to differentiate SIF responses for different vegetation types from a heterogeneous land-use area during drought conditions.

5. Conclusions

This study employed the satellite-based SIF measurements acquired from the recent OCO-2 satellite to study the impact of the 2018 European hotter drought on terrestrial ecosystems. Evidently, OCO-2 SIF displayed the spatial and temporal dynamics of the 2018 European drought across different vegetation types (agricultural area, broadleaved forest, coniferous forest, and mixed forest). Our results show that the agricultural areas were severely affected by the 2018 European hotter drought. While SIF of forests showed a less strong reduction, legacy effects may become visible in the next years and thus, we recommend to closely monitor their behavior. In general, the impact of the heatwave in Central Europe during July-August showed an overall 31% decrease in SIF compared to the reference mean. The SIF variation was closely explained by fPAR variation during non-stressed conditions. However, during water-stress conditions (drought), the SIF variation was attributed to variation in SIFyield. Despite few technical limitations of the OCO-2 SIF measurement such as the 16-days repeat cycle, it provides an excellent potential to study large-scale vegetation fluorescence variation at high spatial resolution and can improve our understanding of changes in ecosystem productivity during extreme events. Furthermore, owing to its direct origin from chlorophyll, OCO-2 SIF is sensitive to both physiological and structural changes in plants and can serve as a complementary dataset to MODIS's vegetation indices (NDVI/EVI). Further application of OCO-2 SIF may include process-based SCOPE modeling to understand the variation of complex fluorescence yield due to different environmental stress, as well as its combination with the XCO2 data (main product of OCO-2 satellite) to study regional carbon budgets.

Supplementary Materials: The following are available online at www.mdpi.com/xxx/s1, Figure S1: title, Table S1: title, Video S1: title.

Author Contributions: **A.S:** Conceptualization, Methodology, Software, Writing-Original Draft, Formal Analysis, Visualization, Funding acquisition. **J.C:** Conceptualization, Methodology, Writing – Review & Editing, Resources, Supervision, Funding acquisition, Project administration. **S.B:** Conceptualization, Writing – Review & Editing. **A.B:** Conceptualization, Methodology, Writing – Review & Editing. **A.O.C:** Visualization, Resources. **C.S.Z:** Methodology, Writing – Review & Editing. **A.R:** Conceptualization, Methodology, Writing – Review & Editing, Supervision, Funding acquisition.

Funding: "This research was funded by Deutscher Akademischer Austauschdienst (DAAD), funding programme ID: India IIT Master Sandwich Programme (IIT), 2018 (57434206)" and "The APC was funded by Technical University of Munich - Institute for Advanced Study through the German Excellence Initiative and the European Union Seventh Framework Program under Grant Nr. 291763 and in part by the German Research Foundation (DFG) under Grant Nr. 419317138".

Acknowledgments: The authors would like to immensely thank the OCO-2 team for providing such a valuable dataset. The authors would like to extend its gratitude to Deutscher Akademischer Austauschdienst (DAAD) and Centre of Rivers Atmosphere and Land Sciences (CORAL), IIT Kharagpur, for funding the research stay at Technical University of Munich and to Mr. Phillip Papastefanou for his discussion about different drought induced plant physiological responses.

Conflicts of Interest: Declare conflicts of interest or state "The authors declare no conflict of interest."

Appendix A

To show that our way of sampling is robust, we have compared the most recent version of spatially downscaled GOME-2 SIF (8 day GOME-2 downscaled SIF of 0.05*0.05 resolution at 740nm; [97]) means with the OCO-2 SIF means. The percentage change in 2018 from both downscaled GOME-2 SIF (GSIF) and OCO-2 was comparable (Table A1). This shows that although OCO-2 does not have a fixed revisit time. Aggregated mean values over a continental scale are robust for multi-year comparison.

Table A1. Comparison of percentage change in GSIF [97] and OCO-2 SIF measurement (used in this study) in 2018 in comparison to Mean (2015-2017) year for three different areas.

	% Change from Mean	
Aggregated Area	**GSIF**	**OCO-2 measurements**
Heatwave	-28.91	-31.04
Spring-Drought Area	6.20	4.90
Summer-Drought Area	-10.98	-12.65

Preprints (www.preprints.org) | NOT PEER-REVIEWED | Posted: 14 August 2020 doi:10.20944/preprints202008.0327.v1

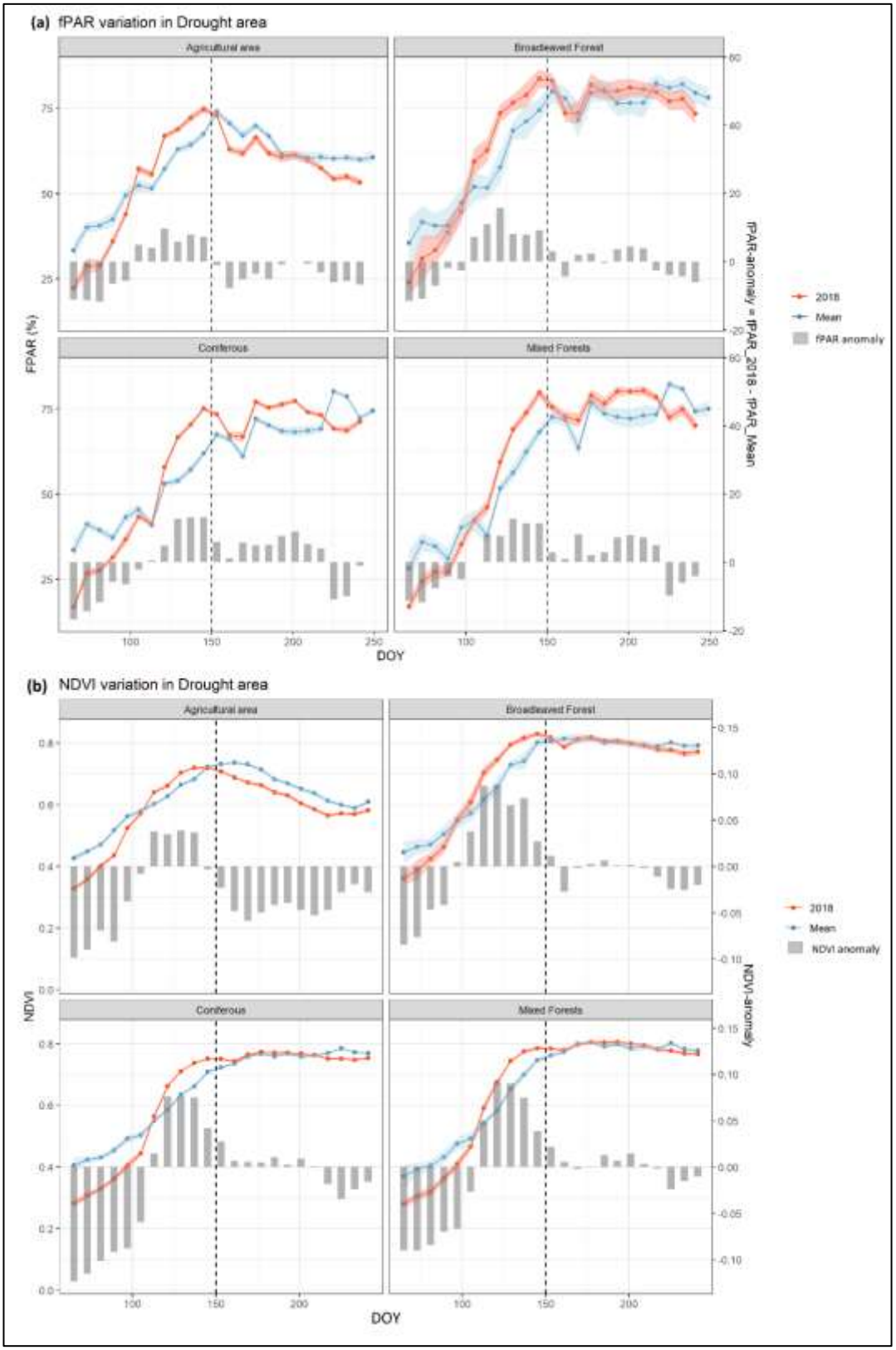

Figure A1. Variation of (a) fPAR and (b) NDVI for drought area across different vegetation types as observed from MODIS fPAR product (MYD15A2H) version 6 and MODIS NDVI product (MOD/MYD13Q1) version 6. The fPAR and NDVI values are sampled from the OCO-2 SIF footprint and are spatially and temporally averaged for three previous years (2015-2017; 'Mean') and year 2018 ('2018'). fPAR anomalies (fPAR_2018 – fPAR_Mean) and NDVI anomalies (NDVI_2018 – NDVI_Mean) are represented by gray bars. The left and right side of vertical solid line represents spring and summer season, respectively.

References

1. IPCC *Summary for Poliymakers*; 2018; ISBN 9789291691517.
2. Dosio, A.; Mentaschi, L.; Fischer, E.M.; Wyser, K. Extreme heat waves under 1.5 °c and 2 °c global warming. *Environ. Res. Lett.* **2018**, doi:10.1088/1748-9326/aab827.
3. Lhotka, O.; Kyselý, J.; Farda, A. Climate change scenarios of heat waves in Central Europe and their uncertainties. *Theor. Appl. Climatol.* **2018**, doi:10.1007/s00704-016-2031-3.
4. Van Loon, A.F.; Gleeson, T.; Clark, J.; Van Dijk, A.I.J.M.; Stahl, K.; Hannaford, J.; Di Baldassarre, G.; Teuling, A.J.; Tallaksen, L.M.; Uijlenhoet, R.; et al. Drought in the Anthropocene. *Nat. Geosci.* 2016.
5. Allen, C.D.; Breshears, D.D.; McDowell, N.G. On underestimation of global vulnerability to tree mortality and forest die-off from hotter drought in the Anthropocene. *Ecosphere* **2015**, doi:10.1890/ES15-00203.1.
6. Buras, A.; Rammig, A.; Zang, C.S. Quantifying impacts of the 2018 drought on European ecosystems in comparison to 2003. *Biogeosciences* **2020**, doi:10.5194/bg-17-1655-2020.
7. Shekhar, Ankit; Bhattacharjee, Shrutilipi; Chen, Jia; Rammig, A. Spring-summer variation analysis in OCO-2's Solar Induced Fluorescence during the European heatwave in 2018. In Proceedings of the Geophysical Research Abstracts; 2019.
8. Heatwave in northern Europe, summer 2018 Available online: https://www.worldweatherattribution.org/attribution-of-the-2018-heat-in-northern-europe/.
9. Ciais, P.; Reichstein, M.; Viovy, N.; Granier, A.; Ogée, J.; Allard, V.; Aubinet, M.; Buchmann, N.; Bernhofer, C.; Carrara, A.; et al. Europe-wide reduction in primary productivity caused by the heat and drought in 2003. *Nature* **2005**, *437*, 529–533, doi:10.1038/nature03972.
10. Phillips, O.L.; Aragão, L.E.O.C.; Lewis, S.L.; Fisher, J.B.; Lloyd, J.; López-González, G.; Malhi, Y.; Monteagudo, A.; Peacock, J.; Quesada, C.A.; et al. Drought sensitivity of the amazon rainforest. *Science (80-.).* **2009**, doi:10.1126/science.1164033.
11. Beer, C.; Reichstein, M.; Tomelleri, E.; Ciais, P.; Jung, M.; Carvalhais, N.; Rödenbeck, C.; Arain, M.A.; Baldocchi, D.; Bonan, G.B.; et al. Terrestrial gross carbon dioxide uptake: Global distribution and covariation with climate. *Science (80-.).* **2010**, doi:10.1126/science.1184984.
12. Lawrence, D.M.; Oleson, K.W.; Flanner, M.G.; Thornton, P.E.; Swenson, S.C.; Lawrence, P.J.; Zeng, X.; Yang, Z.-L.; Levis, S.; Sakaguchi, K.; et al. Parameterization improvements and functional and structural advances in Version 4 of the Community Land Model. *J. Adv. Model. Earth Syst.* **2011**, doi:10.1029/2011ms000045.
13. Li, X.; Xiao, J.; He, B. Chlorophyll fluorescence observed by OCO-2 is strongly related to gross primary productivity estimated from flux towers in temperate forests. *Remote Sens. Environ.* **2018**, *204*, 659–671, doi:10.1016/j.rse.2017.09.034.
14. Smith, W.K.; Biederman, J.A.; Scott, R.L.; Moore, D.J.P.; He, M.; Kimball, J.S.; Yan, D.; Hudson, A.; Barnes, M.L.; MacBean, N.; et al. Chlorophyll Fluorescence Better Captures Seasonal and Interannual Gross Primary Productivity Dynamics Across Dryland Ecosystems of Southwestern North America. *Geophys. Res. Lett.* **2018**, *45*, 748–757, doi:10.1002/2017GL075922.
15. Sun, Y.; Frankenberg, C.; Wood, J.D.; Schimel, D.S.; Jung, M.; Guanter, L.; Drewry, D.T.; Verma, M.; Porcar-Castell, A.; Griffis, T.J.; et al. OCO-2 advances photosynthesis observation from space via solar-induced chlorophyll fluorescence. *Science (80-.).* **2017**, *358*, doi:10.1126/science.aam5747.
16. Xiao, J.; Li, X.; He, B.; Arain, M.A.; Beringer, J.; Desai, A.R.; Emmel, C.; Hollinger, D.Y.; Krasnova, A.; Mammarella, I.; et al. Solar-induced chlorophyll fluorescence exhibits a universal relationship with gross

primary productivity across a wide variety of biomes. *Glob. Chang. Biol.* **2019**, *25*, e4–e6, doi:10.1111/gcb.14565.

17. Yang, X.; Tang, J.; Mustard, J.F.; Lee, J.E.; Rossini, M.; Joiner, J.; Munger, J.W.; Kornfeld, A.; Richardson, A.D. Solar-induced chlorophyll fluorescence that correlates with canopy photosynthesis on diurnal and seasonal scales in a temperate deciduous forest. *Geophys. Res. Lett.* **2015**, doi:10.1002/2015GL063201.
18. Baker, N.R. Chlorophyll Fluorescence: A Probe of Photosynthesis In Vivo. *Annu. Rev. Plant Biol.* **2008**, doi:10.1146/annurev.arplant.59.032607.092759.
19. Meroni, M.; Rossini, M.; Guanter, L.; Alonso, L.; Rascher, U.; Colombo, R.; Moreno, J. Remote sensing of solar-induced chlorophyll fluorescence: Review of methods and applications. *Remote Sens. Environ.* **2009**, *113*, 2037–2051, doi:10.1016/j.rse.2009.05.003.
20. Zarco-Tejada, P.J.; Morales, A.; Testi, L.; Villalobos, F.J. Spatio-temporal patterns of chlorophyll fluorescence and physiological and structural indices acquired from hyperspectral imagery as compared with carbon fluxes measured with eddy covariance. *Remote Sens. Environ.* **2013**, doi:10.1016/j.rse.2013.02.003.
21. Frankenberg, C.; Fisher, J.B.; Worden, J.; Badgley, G.; Saatchi, S.S.; Lee, J.E.; Toon, G.C.; Butz, A.; Jung, M.; Kuze, A.; et al. New global observations of the terrestrial carbon cycle from GOSAT: Patterns of plant fluorescence with gross primary productivity. *Geophys. Res. Lett.* **2011**, *38*, 1–6, doi:10.1029/2011GL048738.
22. Guanter, L.; Zhang, Y.; Jung, M.; Joiner, J.; Voigt, M.; Berry, J.A.; Frankenberg, C.; Huete, A.R.; Zarco-Tejada, P.; Lee, J.E.; et al. Global and time-resolved monitoring of crop photosynthesis with chlorophyll fluorescence. *Proc. Natl. Acad. Sci. U. S. A.* **2014**, doi:10.1073/pnas.1320008111.
23. Joiner, J.; Yoshida, Y.; Vasilkov, A.P.; Yoshida, Y.; Corp, L.A.; Middleton, E.M. First observations of global and seasonal terrestrial chlorophyll fluorescence from space. *Biogeosciences* **2011**, *8*, 637–651, doi:10.5194/bg-8-637-2011.
24. Parazoo, N.C.; Bowman, K.; Fisher, J.B.; Frankenberg, C.; Jones, D.B.A.; Cescatti, A.; Pérez-Priego, Ó.; Wohlfahrt, G.; Montagnani, L. Terrestrial gross primary production inferred from satellite fluorescence and vegetation models. *Glob. Chang. Biol.* **2014**, *20*, 3103–3121, doi:10.1111/gcb.12652.
25. Sanders, A.F.J.; Verstraeten, W.W.; Kooreman, M.L.; van Leth, T.C.; Beringer, J.; Joiner, J. Spaceborne sun-induced vegetation fluorescence time series from 2007 to 2015 evaluated with Australian flux tower measurements. *Remote Sens.* **2016**, *8*, 1–24, doi:10.3390/rs8110895.
26. Verma, M.; Schimel, D.; Evans, B.; Frankenberg, C.; Beringer, J.; Drewry, D.T.; Magney, T.; Marang, I.; Hutley, L.; Moore, C.; et al. Effect of environmental conditions on the relationship between solar-induced fluorescence and gross primary productivity at an OzFlux grassland site. *J. Geophys. Res. Biogeosciences* **2017**, *122*, 716–733, doi:10.1002/2016JG003580.
27. Wood, J.D.; Griffis, T.J.; Baker, J.M.; Frankenberg, C.; Verma, M.; Yuen, K. Multiscale analyses of solar-induced florescence and gross primary production. *Geophys. Res. Lett.* **2017**, *44*, 533–541, doi:10.1002/2016GL070775.
28. Zhang, Y.; Guanter, L.; Berry, J.A.; Joiner, J.; van der Tol, C.; Huete, A.; Gitelson, A.; Voigt, M.; Köhler, P. Estimation of vegetation photosynthetic capacity from space-based measurements of chlorophyll fluorescence for terrestrial biosphere models. *Glob. Chang. Biol.* **2014**, doi:10.1111/gcb.12664.
29. Joiner, J.; Yoshida, Y.; Vasilkov, A.P.; Yoshida, Y.; Corp, L.A.; Middleton, E.M. First observations of global and seasonal terrestrial chlorophyll fluorescence from space. *Biogeosciences* **2011**, *8*, 637–651, doi:10.5194/bg-8-637-2011.

30. Frankenberg, C.; Fisher, J.B.; Worden, J.; Badgley, G.; Saatchi, S.S.; Lee, J.E.; Toon, G.C.; Butz, A.; Jung, M.; Kuze, A.; et al. New global observations of the terrestrial carbon cycle from GOSAT: Patterns of plant fluorescence with gross primary productivity. *Geophys. Res. Lett.* **2011**, *38*, 1–6, doi:10.1029/2011GL048738.
31. Guanter, L.; Zhang, Y.; Jung, M.; Joiner, J.; Voigt, M.; Berry, J.A.; Frankenberg, C.; Huete, A.R.; Zarco-Tejada, P.; Lee, J.E.; et al. Global and time-resolved monitoring of crop photosynthesis with chlorophyll fluorescence. *Proc. Natl. Acad. Sci. U. S. A.* **2014**, *111*, doi:10.1073/pnas.1320008111.
32. Frankenberg, C.; O'Dell, C.; Berry, J.; Guanter, L.; Joiner, J.; Köhler, P.; Pollock, R.; Taylor, T.E. Prospects for chlorophyll fluorescence remote sensing from the Orbiting Carbon Observatory-2. *Remote Sens. Environ.* **2014**, *147*, 1–12, doi:10.1016/j.rse.2014.02.007.
33. Lee, J.E.; Frankenberg, C.; Van Der Tol, C.; Berry, J.A.; Guanter, L.; Boyce, C.K.; Fisher, J.B.; Morrow, E.; Worden, J.R.; Asefi, S.; et al. Forest productivity and water stress in Amazonia: Observations from GOSAT chlorophyll fluorescence. *Tohoku J. Exp. Med.* **2013**, *230*, doi:10.1098/rspb.2013.0171.
34. Yoshida, Y.; Joiner, J.; Tucker, C.; Berry, J.; Lee, J.E.; Walker, G.; Reichle, R.; Koster, R.; Lyapustin, A.; Wang, Y. The 2010 Russian drought impact on satellite measurements of solar-induced chlorophyll fluorescence: Insights from modeling and comparisons with parameters derived from satellite reflectances. *Remote Sens. Environ.* **2015**, *166*, 163–177, doi:10.1016/j.rse.2015.06.008.
35. Sun, Y.; Fu, R.; Dickinson, R.; Joiner, J.; Frankenberg, C.; Gu, L.; Xia, Y.; Fernando, N. Drought onset mechanisms revealed by satellite solar-induced chlorophyll fluorescence: Insights from two contrasting extreme events. *J. Geophys. Res. G Biogeosciences* **2015**, *120*, 2427–2440, doi:10.1002/2015JG003150.
36. Koren, G.; Van Schaik, E.; Araújo, A.C.; Boersma, K.F.; Gärtner, A.; Killaars, L.; Kooreman, M.L.; Kruijt, B.; Van Der Laan-Luijkx, I.T.; Von Randow, C.; et al. Widespread reduction in sun-induced fluorescence from the Amazon during the 2015/2016 El Niño. *Philos. Trans. R. Soc. B Biol. Sci.* **2018**, *373*, doi:10.1098/rstb.2017.0408.
37. Zhang, Y.; Joiner, J.; Hamed Alemohammad, S.; Zhou, S.; Gentine, P. A global spatially contiguous solar-induced fluorescence (CSIF) dataset using neural networks. *Biogeosciences* **2018**, *15*, 5779–5800, doi:10.5194/bg-15-5779-2018.
38. Vicente-Serrano, S.M.; Beguería, S.; López-Moreno, J.I. A multiscalar drought index sensitive to global warming: The standardized precipitation evapotranspiration index. *J. Clim.* **2010**, doi:10.1175/2009JCLI2909.1.
39. NOAA National Centers for Environmental Information *State of the Climate: Global Climate Report for August 2018*; 2018;
40. NOAA National Centers for Environmental Information *State of the Climate: Global Climate Report for July 2018*; 2018;
41. Damm, A.; Elber, J.; Erler, A.; Gioli, B.; Hamdi, K.; Hutjes, R.; Kosvancova, M.; Meroni, M.; Miglietta, F.; Moersch, A.; et al. Remote sensing of sun-induced fluorescence to improve modeling of diurnal courses of gross primary production (GPP). *Glob. Chang. Biol.* **2010**, doi:10.1111/j.1365-2486.2009.01908.x.
42. Damm, A.; Guanter, L.; Paul-Limoges, E.; van der Tol, C.; Hueni, A.; Buchmann, N.; Eugster, W.; Ammann, C.; Schaepman, M.E. Far-red sun-induced chlorophyll fluorescence shows ecosystem-specific relationships to gross primary production: An assessment based on observational and modeling approaches. *Remote Sens. Environ.* **2015**, doi:10.1016/j.rse.2015.06.004.
43. Frankenberg, C.; Berry, J. *Solar Induced Chlorophyll Fluorescence: Origins, Relation to Photosynthesis and Retrieval*; Elsevier, 2018;

44. Frankenberg, C.; Butz, A.; Toon, G.C. Disentangling chlorophyll fluorescence from atmospheric scattering effects in O2 A-band spectra of reflected sun-light. *Geophys. Res. Lett.* **2011**, doi:10.1029/2010GL045896.
45. Sun, Y.; Frankenberg, C.; Jung, M.; Joiner, J.; Guanter, L.; Köhler, P.; Magney, T. Overview of Solar-Induced chlorophyll Fluorescence (SIF) from the Orbiting Carbon Observatory-2: Retrieval, cross-mission comparison, and global monitoring for GPP. *Remote Sens. Environ.* **2018**, *209*, 808–823, doi:10.1016/j.rse.2018.02.016.
46. Shekhar, A.; Chen, J.; Paetzold, J.C.; Dietrich, F.; Zhao, X.; Bhattacharjee, S.; Ruisinger, V.; Wofsy, S.C. Anthropogenic CO2 emissions assessment of Nile Delta using XCO2 and SIF data from OCO-2 satellite. *Environ. Res. Lett.* **2020**, doi:10.1088/1748-9326/ab9cfe.
47. Frankenberg, C. Solar Induced Chlorophyll Fluorescence: OCO-2 Lite Files (B7000) User Guide. **2015**, 10.
48. Zhang, Z.; Zhang, Y.; Joiner, J.; Migliavacca, M. Angle matters: Bidirectional effects impact the slope of relationship between gross primary productivity and sun-induced chlorophyll fluorescence from Orbiting Carbon Observatory-2 across biomes. *Glob. Chang. Biol.* **2018**, *24*, 5017–5020, doi:10.1111/gcb.14427.
49. Goulas, Y.; Daumard, F.; Ounis, A.; Rhoul, C.; Lopez, M.L.; Moya, I. Monitoring the diurnal time course of vegetation dynamics with geostationary observations: The gflex project. In Proceedings of the Workshop on Hyperspectral Image and Signal Processing, Evolution in Remote Sensing; 2014.
50. Yan, K.; Park, T.; Yan, G.; Chen, C.; Yang, B.; Liu, Z.; Nemani, R.R.; Knyazikhin, Y.; Myneni, R.B. Evaluation of MODIS LAI/FPAR product collection 6. Part 1: Consistency and improvements. *Remote Sens.* **2016**, doi:10.3390/rs8050359.
51. Yan, K.; Park, T.; Yan, G.; Liu, Z.; Yang, B.; Chen, C.; Nemani, R.R.; Knyazikhin, Y.; Myneni, R.B. Evaluation of MODIS LAI/FPAR product collection 6. Part 2: Validation and intercomparison. *Remote Sens.* **2016**, doi:10.3390/rs8060460.
52. Knyazikhin, Y.; Myneni, R.B.; Privette, J.L.; Running, S.W.; Nemani, R.; Zhang, Y.; Tian, Y.; Wang, Y.; Morissette, J.T.; Glassy, J.; et al. *MODIS Leaf Area Index (LAI) and Fraction of Photosynthetically Active Radiation Absorbed by Vegetation (FPAR) Product (MOD15) Algorithm Theoretical Basis Document*; 1999;
53. Solano, R.; Didan, K.; Jacobson, A.; Huete, A. MODIS Vegetation Index User ' s Guide (MOD13 Series). *Univ. Arizona* **2010**.
54. Büttner, G.; Kosztra, B. CLC2018 Technical Guidelines. **2017**, 0–60.
55. Wable, P.S.; Jha, M.K.; Shekhar, A. Comparison of Drought Indices in a Semi-Arid River Basin of India. *Water Resour. Manag.* **2019**, doi:10.1007/s11269-018-2089-z.
56. Nam, W.H.; Hayes, M.J.; Svoboda, M.D.; Tadesse, T.; Wilhite, D.A. Drought hazard assessment in the context of climate change for South Korea. *Agric. Water Manag.* **2015**, doi:10.1016/j.agwat.2015.06.029.
57. Zang, C.S.; Buras, A.; Esquivel-Muelbert, A.; Jump, A.S.; Rigling, A.; Rammig, A. Standardized drought indices in ecological research: Why one size does not fit all. *Glob. Chang. Biol.* **2019**, 1–3, doi:10.1111/gcb.14809.
58. Ionita, M.; Tallaksen, L.M.; Kingston, D.G.; Stagge, J.H.; Laaha, G.; Van Lanen, H.A.J.; Scholz, P.; Chelcea, S.M.; Haslinger, K. The European 2015 drought from a climatological perspective. *Hydrol. Earth Syst. Sci.* 2017.
59. Dong, B.; Sutton, R.; Shaffrey, L.; Wilcox, L. The 2015 European heat wave. In *Bulletin of the American Meteorological Society*; 2016.
60. McCornack, R.L. Extended Tables of the Wilcoxon Matched Pair Signed Rank Statistic. *J. Am. Stat. Assoc.*

1965, doi:10.1080/01621459.1965.10480835.

61. KMI *"Klimatologisch Maandoverzicht juli 2018" (PDF) (in Dutch).*; 2018;
62. KNMI *"KNMI - Hittegolf". www.knmi.nl*; 2019;
63. Danmarks Meteorologiske Institut. *"Juni bliver den varmeste og solrigeste i 26 år" (in Danish)*; 2018;
64. DWD *Deutscher Wetterdienst. 1 August 2018*; 2018;
65. R Development Core Team, R. R: A Language and Environment for Statistical Computing. *R Found. Stat. Comput.* 2011, *1*, 409.
66. Wickham, H. *ggplot2: elegant graphics for data analysis*; 2016; ISBN 978-3-319-24275-0.
67. Wickham, H.; Francois, R. dplyr: A Grammar of Data Manipulation. *R Packag. version 0.4.2.* **2015**.
68. Shekhar, A.; Shapiro, C.A. What do meteorological indices tell us about a long-term tillage study? *Soil Tillage Res.* **2019**, *193*, 161–170, doi:10.1016/j.still.2019.06.004.
69. Paul-Limoges, E.; Damm, A.; Hueni, A.; Liebisch, F.; Eugster, W.; Schaepman, M.E.; Buchmann, N. Effect of environmental conditions on sun-induced fluorescence in a mixed forest and a cropland. *Remote Sens. Environ.* **2018**, doi:10.1016/j.rse.2018.10.018.
70. Miralles, D.G.; Teuling, A.J.; Van Heerwaarden, C.C.; De Arellano, J.V.G. Mega-heatwave temperatures due to combined soil desiccation and atmospheric heat accumulation. *Nat. Geosci.* **2014**, doi:10.1038/ngeo2141.
71. Sippel, S.; Forkel, M.; Rammig, A.; Thonicke, K.; Flach, M.; Heimann, M.; Otto, F.E.L.; Reichstein, M.; Mahecha, M.D. Contrasting and interacting changes in simulated spring and summer carbon cycle extremes in European ecosystems. *Environ. Res. Lett.* **2017**, doi:10.1088/1748-9326/aa7398.
72. Porcar-Castell, A.; Tyystjärvi, E.; Atherton, J.; Van Der Tol, C.; Flexas, J.; Pfündel, E.E.; Moreno, J.; Frankenberg, C.; Berry, J.A. Linking chlorophyll a fluorescence to photosynthesis for remote sensing applications: Mechanisms and challenges. *J. Exp. Bot.* **2014**, *65*, 4065–4095, doi:10.1093/jxb/eru191.
73. Crausbay, S.D.; Ramirez, A.R.; Carter, S.L.; Cross, M.S.; Hall, K.R.; Bathke, D.J.; Betancourt, J.L.; Colt, S.; Cravens, A.E.; Dalton, M.S.; et al. Defining ecological drought for the twenty-first century. *Bull. Am. Meteorol. Soc.* **2017**, doi:10.1175/BAMS-D-16-0292.1.
74. Sippela, S.; Zscheischlerb, J.; Reichsteina, M. Ecosystem impacts of climate extremes crucially depend on the timing. *Proc. Natl. Acad. Sci. U. S. A.* 2016.
75. Chen, J.; Franklin, J.F.; Spies, T.A. Contrasting microclimates among clearcut, edge, and interior of old-growth Douglas-fir forest. *Agric. For. Meteorol.* **1993**, doi:10.1016/0168-1923(93)90061-L.
76. Chen, J.; Saunders, S.C.; Crow, T.R.; Naiman, R.J.; Brosofske, K.D.; Mroz, G.D.; Brookshire, B.L.; Franklin, J.F. Microclimate in forest ecosystem and landscape ecology: Variations in local climate can be used to monitor and compare the effects of different management regimes. *Bioscience* **1999**, doi:10.2307/1313612.
77. Young, A.; Mitchell, N. Microclimate and vegetation edge effects in a fragmented podocarp-broadleaf forest in New Zealand. *Biol. Conserv.* **1994**, doi:10.1016/0006-3207(94)90010-8.
78. Krishnan, P.; Black, T.A.; Grant, N.J.; Barr, A.G.; Hogg, E. (Ted) H.; Jassal, R.S.; Morgenstern, K. Impact of changing soil moisture distribution on net ecosystem productivity of a boreal aspen forest during and following drought. *Agric. For. Meteorol.* **2006**, doi:10.1016/j.agrformet.2006.07.002.
79. Anderegg, W.R.L.; Schwalm, C.; Biondi, F.; Camarero, J.J.; Koch, G.; Litvak, M.; Ogle, K.; Shaw, J.D.; Shevliakova, E.; Williams, A.P.; et al. Pervasive drought legacies in forest ecosystems and their implications for carbon cycle models. *Science (80-.).* **2015**, doi:10.1126/science.aab1833.
80. Buras, A.; Schunk, C.; Zeitrg, C.; Herrmann, C.; Kaiser, L.; Lemme, H.; Straub, C.; Taeger, S.; Gößwein, S.; Klemmt, H.J.; et al. Are Scots pine forest edges particularly prone to drought-induced mortality?

Environ. Res. Lett. **2018**, doi:10.1088/1748-9326/aaa0b4.

81. Dobrowski, S.Z.; Pushnik, J.C.; Zarco-Tejada, P.J.; Ustin, S.L. Simple reflectance indices track heat and water stress-induced changes in steady-state chlorophyll fluorescence at the canopy scale. *Remote Sens. Environ.* **2005**, doi:10.1016/j.rse.2005.05.006.
82. Wang, S.; Huang, C.; Zhang, L.; Lin, Y.; Cen, Y.; Wu, T. Monitoring and assessing the 2012 drought in the great plains: Analyzing satellite-retrieved solar-induced chlorophyll fluorescence, drought indices, and gross primary production. *Remote Sens.* **2016**, *8*, doi:10.3390/rs8020061.
83. De Boeck, H.J.; Verbeeck, H. Drought-associated changes in climate and their relevance for ecosystem experiments and models. *Biogeosciences* **2011**, doi:10.5194/bg-8-1121-2011.
84. Fischer, E.M.; Seneviratne, S.I.; Vidale, P.L.; Lüthi, D.; Schär, C. Soil moisture-atmosphere interactions during the 2003 European summer heat wave. *J. Clim.* **2007**, doi:10.1175/JCLI4288.1.
85. Chaves, M.M. Effects of water deficits on carbon assimilation. *J. Exp. Bot.* 1991.
86. Keenan, T.; Sabate, S.; Gracia, C. The importance of mesophyll conductance in regulating forest ecosystem productivity during drought periods. *Glob. Chang. Biol.* **2010**, doi:10.1111/j.1365-2486.2009.02017.x.
87. Bréda, N.; Huc, R.; Granier, A.; Dreyer, E. Temperate forest trees and stands under severe drought: A review of ecophysiological responses, adaptation processes and long-term consequences. *Ann. For. Sci.* 2006.
88. Porcar-Castell, A.; Tyystjärvi, E.; Atherton, J.; Van Der Tol, C.; Flexas, J.; Pfündel, E.E.; Moreno, J.; Frankenberg, C.; Berry, J.A. Linking chlorophyll a fluorescence to photosynthesis for remote sensing applications: Mechanisms and challenges. *J. Exp. Bot.* 2014.
89. Castro, A.O.; Chen, J.; Zang, C.S.; Shekhar, A.; Jimenez, J.C.; Bhattacharjee, S.; Kindu, M.; Morales, V.H.; Rammig, A. OCO-2 solar-induced chlorophyll fluorescence variability across ecoregions of the Amazon basin and the extreme drought effects of El Niño (2015-2016). *Remote Sens.* **2020**, doi:10.3390/rs12071202.
90. Kasahara, M.; Kagawa, T.; Olkawa, K.; Suetsugu, N.; Miyao, M.; Wada, M. Chlomplast avoidance movement reduces photodamage in plants. *Nature* **2002**, doi:10.1038/nature01213.
91. Field, C.B. Ecological Scaling of Carbon Gain to Stress and Resource Availability. In *Response of Plants to Multiple Stresses*; Elsevier, 1991; pp. 35–65 ISBN 9780125053556.
92. Flexas, J.; Medrano, H. Drought-inhibition of photosynthesis in C3 plants: Stomatal and non-stomatal limitations revisited. *Ann. Bot.* **2002**, doi:10.1093/aob/mcf027.
93. Paul-Limoges, E.; Damm, A.; Hueni, A.; Liebisch, F.; Eugster, W.; Schaepman, M.E.; Buchmann, N. Effect of environmental conditions on sun-induced fluorescence in a mixed forest and a cropland. *Remote Sens. Environ.* **2018**, *219*, 310–323, doi:10.1016/j.rse.2018.10.018.
94. Peguero-Pina, J.J.; Morales, F.; Flexas, J.; Gil-Pelegrín, E.; Moya, I. Photochemistry, remotely sensed physiological reflectance index and de-epoxidation state of the xanthophyll cycle in Quercus coccifera under intense drought. *Oecologia* **2008**, doi:10.1007/s00442-007-0957-y.
95. Yang, P.; van der Tol, C. Linking canopy scattering of far-red sun-induced chlorophyll fluorescence with reflectance. *Remote Sens. Environ.* **2018**, *209*, 456–467, doi:10.1016/j.rse.2018.02.029.
96. Zeng, Y.; Badgley, G.; Dechant, B.; Ryu, Y.; Chen, M.; Berry, J.A. A practical approach for estimating the escape ratio of near-infrared solar-induced chlorophyll fluorescence. *Remote Sens. Environ.* **2019**, doi:10.1016/j.rse.2019.05.028.
97. Duveiller, G.; Filipponi, F.; Walther, S.; Köhler, P.; Frankenberg, C.; Guanter, L.; Cescatti, A. A spatially downscaled sun-induced fluorescence global product for enhanced monitoring of vegetation productivity. *Earth Syst. Sci. Data* **2020**, doi:10.5194/essd-12-1101-2020.